Inorg. Chem. **2007**, *46*, 11036–11047

Inorganic Chemistry

Article

Fast Synthesis of ZnO Nanostructures by Laser-Induced Decomposition of Zinc Acetylacetonate

Christian Fauteux,* Rémi Longtin, Joseph Pegna, and Daniel Therriault

Micro- and Nanofabrication Laboratory by Direct-Write, Center for Applied Research on Polymers and Composites (CREPEC), Department of Mechanical Engineering, École Polytechnique de Montréal, Box 6079, Station A, Montréal, QC H3C 3A7, Canada

Received May 11, 2007

A CO_2 laser ($\lambda = 10.6$ μm) was used to heat a solution of water and alcohol saturated by $Zn(AcAc)_2$ on a fused quartz substrate in open air. After only a few seconds of irradiation, various zinc oxide (ZnO) nanostructures including nanorods and nanowires are formed near the center of the irradiated zone, surrounded by a porous thin film of ZnO nanoparticles. The type of structures produced and their localization on the substrate can be varied by selecting adequate irradiation time and laser power ranges. The deposits have been analyzed using SEM, TEM, EDS, XRD, and Raman spectroscopy, revealing that the nanorods (aspect ratio ∼6) and nanowires (aspect ratio ∼94) are single-crystalline structures which grow along the *c* axis of wurtzite ZnO. The nanoparticles are also single-crystalline and have an average diameter of 16 nm. A qualitative model for nanostructure growth is proposed, based on previous studies of aqueous solution and hydrothermal processing.

Introduction

Presenting very attractive engineering properties like large exciton binding energy (60 meV), photoluminescence, and piezoelectricity while being easily synthesizable in a plethora of different morphologies in single-crystal form, nanostructured zinc oxide has become one of the most studied semiconductor nanomaterials of the beginning of the 21st century.[1] Because of their great potential for the fabrication of new devices, in particular for optoelectronic and gas-sensing applications, 1D ZnO nanostructures have attracted much attention.[2] For example, oriented ZnO microtube arrays have been grown by solution chemistry[3] for bio-/gas sensors and by the microwave heating of Zn powders for field-emission and selective UV light response.[4] UV lasing has been observed from ZnO whiskers[5] and gas-sensing devices,[6] and UV photodiodes[7] were made from multipod-shaped nanorods.

The key process requirements for the successful integration of 1D nanostructures in technological devices are structure alignment and simultaneous control over uniformity, morphology, and dimensions.[8] Notably, this has been achieved by vapor-phase techniques such as thermal evaporation of powders and vapor liquid solid (VLS) growth on patterned catalyst surfaces.[2] The temperatures used for the growth of ZnO nanowires and nanorods by the evaporation of ZnO[9] and Zn powders[10] are between 700 and 1300 °C[11] but can be lowered by using a metal catalyst such as nickel.[12]

Milder process conditions with lower decomposition temperatures and nontoxic reagents are preferable for large-scale industrial applications. The chemical processing route for the production of nanostructured ZnO, be it hydrothermal

---

* To whom correspondence should be addressed. E-mail: christian.fauteux@polymtl.ca. Tel: 514-340-4711-7408. Fax: 514-340-5282.

(1) Wang, Z. L. *J. Phys.: Condens. Matter*. **2004**, *16*, R829.
(2) Yi, G. C.; Wang, C.; Park, W. I. *Semicond. Sci. Technol.* **2005**, *20*, S22.
(3) Vayssieres, L.; Keis, K.; Hagfeldt, A.; Lindquist, S. E. *Chem. Mater.* **2001**, *13*, 4395.
(4) Cheng, J.; Guo, R.; Wang, Q. M. *Appl. Phys. Lett.* **2004**, *85*, 5140.
(5) Wang, Y. G.; Yuen, C.; Lau, S. P.; Yu, S. F.; Tay, B. K. *Chem. Phys. Lett.* **2003**, *377*, 329.
(6) Wang, T. H.; Gao, T. *Appl. Phys. A: Mater. Sci. Process.* **2005**, *80*, 1451.
(7) Newton, M. C.; Firth, S.; Warburton, P. A. *Appl. Phys. Lett.* **2006**, *89*, 072104.
(8) Xia, Y.; Yang, P.; Sun, Y.; Wu, Y.; Mayers, B.; Gates, B.; Yin, Y.; Kim, F.; Yan, H. *Adv. Mater.* **2003**, *15*, 353.
(9) Jie, J.; Wang, G.; Chen, Y.; Han, X.; Wang, Q.; Xu, B. *Appl. Phys. Lett.* **2005**, *86*, 031909.
(10) Zhao, Y. N.; Cao, M. S.; Jin, H. B.; Zhang, L.; Qiu, C. *Scripta Mater.* **2006**, *54*, 2057.
(11) Xing, Y. J.; Xi, Z. H.; Zhang, X. D.; Song, J. H.; Wang, R. M.; Xu, J.; Xue, Z. Q.; Yu, D. P. *Appl. Phys. A: Mater. Sci. Process.* **2005**, *80*, 1527.
(12) Lyu, S. C.; Zhang, Y.; Ruh, H.; Lee, H. J.; Shim, H. W.; Suh, E. K.; Lee, C. J. *Chem. Phys. Lett.* **2002**, *363*, 134.

10.1021/ic700915z CCC: $37.00

processing,[13,14] solution chemistry,[15] or sol-gel,[16] has been extensively traveled and allows low-temperature (between 95 and 250 °C) and catalyst-free growth on flat substrates with greater yields than other methods. The zinc precursors generally used are zinc nitrate ($Zn(NO_3)_2$)[17] or zinc acetate ($Zn(C_2H_3O_2)_2$).[18] Additionally, short-chain polymers,[19] mineralizers such as NaOH[20] and KOH,[21] and additives such as ethylenediamine[22] and hexamethylethylenetetramine[23] have successfully been used to promote the 1D growth of ZnO by hydrothermal reactions. The main drawback of these mild methods is the long processing times. With metal organic chemical vapor deposition (MOCVD) taking from 2 to 4 h and solution or hydrothermal processing taking from hours to days to complete, these methods remain mostly useful for applied research.

We propose here a new laser-assisted technique for the fast surface-bound growth of ZnO nanostructures. As a source of ZnO, we have chosen $Zn(AcAc)_2$ for its low decomposition temperature, ease of use, nontoxicity, and wide availability. Laser thermochemistry provides a swift and simple alternative to the long processing times associated with conventional chemical processing without the need for the complicated multistep procedures and expensive vacuum equipment necessary for MOCVD. The high synthesis temperature of VLS- or VS-type processes is also avoided.

Experimental Methods

Solution Preparation. A quantity of 0.4 g of zinc acetylacetonate hydrate ($Zn(C_5H_7O_2)_2{\cdot}H_2O$, >95% purity, Gelest) was manually mixed with 2 mL of deionized water and 2 mL of denatured ethanol (EtOH 85.47%, MeOH 13.68%, EtOAc 0.85%, VWR) for ~5 min, forming a slurry of 0.355 M of $Zn(AcAc)_2{\cdot}H_2O$. The pH of the solution was measured to be 8.25 using a pHSpear calibrated by a NIST traceable pHTestkit (both Oakton). A few drops of the solution was then transferred to a fused quartz substrate (1 cm × 1 cm × 1.15 mm, Ted Pella) using a standard dropper. The average drop radius was 5 mm, the average drop height at the center was 1.2 mm, and the average drop height at 2 mm from the center was 1.06 mm (measured using a CCD camera coupled to a microscope). The substrate had previously been cleaned in a hot ultrasonic bath using the following procedure: 15 min in ethanol, 15 min in DI water, and 15 min in acetone. Finally, to remove the acetone, the substrates were individually submitted to a heated air flow at 200 °C for 3 min. Since $Zn(AcAc)_2$ is hydrophobic (solubility of 7 g/L in water), it partially precipitated on the substrate, remaining covered by a film of solution.

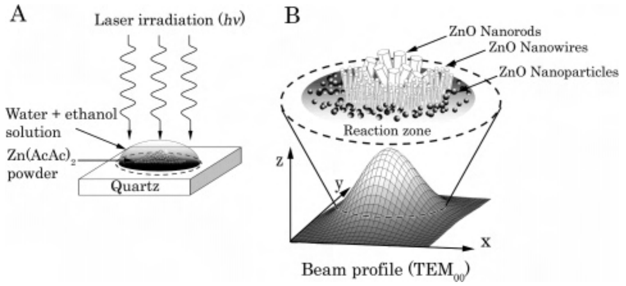

Figure 1. Schematic depiction of the synthesis process. (A) Laser-induced decomposition of precursor solution. (B) Detail of the reaction zone with the different nanostructures obtained.

Laser Decomposition. A precipitate-covered substrate was placed on a stainless-steel substrate holder, and the center was irradiated by an unfocused CO_2 laser (coherent DEOS 100L, $\lambda = 10.6\ \mu m$, waist = 4 mm, aligned by beam injector from ULO) in open air ($T = 23$ °C, low humidity) with an incidence angle of 45° (see Figure 1 for an artistic representation of the synthesis process and its products). The laser was operated in the first transverse electromagnetic mode (TEM_{00}). The laser was turned on less than 5 s after the solution was placed on the substrate. The total substrate area irradiated by laser light was approximately 12 mm^2. The irradiation times investigated ranged from 2 to 10 s, and the laser power was varied from 5 to 30 W, providing light intensities between 40 W/cm^2 (5 W, 10 s) and 239 W/cm^2 (30 W, 10 s).

Characterization. The samples were first observed using an environmental scanning electron microscope (Quanta 200 FEG, FEI Company) equipped with an energy dispersive spectroscopy (EDS) X-ray spectrometer (Genesis 2000, XMS System 60 with a Sapphire Si:Li Detector, EDAX). A field-effect transmission electron microscope (FEG-TEM, Jeol JEM-2100F, 200 kV) with a Gatan Ultrascan 1000 TEM camera was then used to obtain selective area electron diffraction patterns (SAED) and high-resolution TEM (HRTEM) images. The TEM samples were prepared by removing a part of the deposit in the center of the reaction zone using tweezers and by gently rubbing them on TEM grids covered by a carbon film (400 mesh). SEM and TEM image analysis was done using the *ImagePro*, version 5.1, AMS software (Mediacybernetics). X-ray EDS spectra were also taken in the TEM (Inca detector, Oxford instruments) to obtain elemental information on the samples. Quantification was done using the INCA microanalysis suite (Oxford instruments), the Genesis Spectrum utilities (SEM Quant ZAF, Version 3.60, EDAX), and commercial ZnO powder as a reference sample (200 mesh, Alfa Aesar, 99.9% ZnO).

For more general crystallographic information, X-ray diffraction (XRD) patterns of the whole samples were taken using a Philips X'PERT diffractometer equipped with a Cu Kα X-ray source ($\lambda = 1.541$ Å). The acceleration voltage was 50 kV with a 40 mA current. The detector was scanned from 18° to 70° (2θ) at a speed of 0.01°/sec in the grazing angle mode. The source's incident angle was 1°. Raman spectroscopy was performed using an InVia Raman spectroscope (Renishaw) with a 25 mW Ar+ laser ($\lambda = 514.5$ nm) focused by a 50× lens. With the use of this setup, the spectral resolution was 1 cm^{-1} and the spatial resolution was 1 μm. The peak fitting for the XRD patterns and Raman spectra was done using *WIRE*, version 2.0, software (Renishaw) with a mix of Gaussian and Lorentzian curves. Diffraction pattern and Raman spectra smoothing with a Savitsky-Golay polynomial was used to reduce noise and enhance peaks.

---

(13) Iwasaki, M.; Inubushi, Y.; Ito, S. *J. Mater. Sci. Lett.* **1997**, *16*, 1503.

(14) Ma, X.; Zhang, H.; Ji, Y.; Xu, J.; Yang, D. *Mater. Lett.* **2005**, *59*, 3393.

(15) Su, X.; Zhang, Z.; Wang, Y.; Zhu, M. *J. Phys. D: Appl. Phys.* **2005**, *38*, 3934.

(16) Ahn, S. E.; Lee, J. S.; Kim, H.; Kim, S.; Kang, B. H.; Kim, K. H.; Kim, G. T. *Appl. Phys. Lett.* **2004**, *84*, 5022.

(17) Liu, B.; Zeng, H. C. *J. Am. Chem. Soc.* **2003**, *125*, 4430.

(18) Zhang, X. L.; Kang, Y. S. *Inorg. Chem.* **2006**, *45*, 4186.

(19) Li, Z.; Xiong, Y.; Xie, Y. *Inorg. Chem.* **2003**, *42*, 8105.

(20) Liu, B.; Zeng, H. C. *J. Am. Chem. Soc.* **2003**, *125*, 4430.

(21) Dem'yanets, L. N.; Kostomarov, D. V.; Kuz'mina, I. P. *Inorg. Mater.* **2002**, *38*, 124.

(22) Liu, B.; Zeng, H. C. *Langmuir* **2004**, *20*, 4196.

(23) Greene, L. E.; Yuhas, B. D.; Law, M.; Zitoun, D.; Yang, P. *Inorg. Chem.* **2006**, *45*, 7535.

Results and Discussion

Precursor Selection and Chemistry. $Zn(AcAc)_2$ is a proven single-source precursor for ZnO. It has successfully been used in MOCVD processes to grow aligned hexagonal nanorods and whiskers,[24,25] nanotube arrays,[26] and thin films[27] at temperatures between 500 and 650 °C on various substrates. It has also been recently used in the controlled growth of ZnO nanocrystals in a solution of oleylamine and ethanol[28] and the growth of ZnO whiskers in an oxidizing atmosphere.[29]

The thermal decomposition of $Zn(AcAc)_2 \cdot H_2O$ has been studied since the 1960s when it was found that the main decomposition product when heated at 130 °C was gaseous acetylacetone ($C_5H_8O_2$).[30] Iwasaki et al.[13] mentioned that the addition of water in the solution promotes the ligand exchange reaction between $AcAc^-$ and OH^- and the condensation reaction to produce ZnO particles. Fiddes et al.[31] report that at a temperature $T < 200$ °C, the decomposition of $Zn(AcAc)_2 \cdot H_2O$ in wet conditions is due to a combination of exothermic intramolecular and intermolecular processes (mainly nucleophillic attack of the carbonyl carbon by the oxygen in the coordinated and excess water) while at $T > 200$ °C, a water-enhanced pyrolysis mechanism is likely active. Arii et al.[32] confirm that the decomposition temperature is lowered in a high water vapor pressure environment and suggest that crystalline ZnO can be synthesized at temperatures as low as 110 °C via a two-step mass loss with the following simplified thermal decomposition scheme:

$$Zn(C_5H_7O_2)_2 \cdot H_2O_{(s)} \rightarrow ZnO_{(s)} + 2C_5H_8O_{2(g)} \qquad (1)$$

The driving force behind the sudden formation of ZnO in our experiment is probably the fast vaporization of acetylacetone (boiling point of 140 °C) in ambient air and water vapor (solubility of acetylacetone in water is 16 g/100 mL), which moves the equilibrium of eq 1 to the right and causes an abrupt increase in ZnO.

Laser-Induced Decomposition Process. In this experiment, the laser acted as a localized and very intense energy source for the decomposition of $Zn(AcAc)_2$ in a medium of water/ethanol. When the precursor solution droplet was exposed to the laser beam, the droplet's planar surface was observed to roughly double its size and immediately started to evaporate. Solution evaporation was rapid: around 5 s at 10 W and 2 s at 20 W. Fumes were also produced from the reaction zone. A white deposit was visible on the surface of the substrate after irradiation. When irradiation lasted more than 5 s at powers superior or equal to 15 W, visible light (yellow and orange) was emitted from the reaction zone, which was apparently burning. This resulted in the appearance of brown and black spots. For lower powers, the white deposit became yellow after 8 to 10 s. After irradiation, the deposit's color changed back to white.

Liquid water absorbs the infrared (IR) radiation emitted by a CO_2 laser operating at 10.6 μm to a depth of 16−25 μm.[33] Ethanol does not directly absorb this wavelength, although it can be dissociated in the 9 μm region.[34] Considering that the precursor solution droplet is around 1 mm thick in the irradiated region, the solution will absorb all the energy of the laser beam until it is totally evaporated. If the irradiation time is longer than the evaporation time, the laser will heat up the remaining $Zn(AcAc)_2$ and anneal what was deposited before evaporation for the remaining irradiation time. The photons that are not absorbed by the spatially inhomogeneous deposit will be absorbed by the substrate (90% absorption at 10.6 μm) and subsequently heat the deposit/precursor from below. CO_2 laser annealing of ZnO films in air improves the crystalline quality, induces grain growth, and relaxes stress in thin films.[35]

Laser heating is a very rapid and complex heating event. The laser's Gaussian intensity distribution has been known to induce a Gaussian temperature spatial distribution in a solid.[36] When a laser beam irradiates a thin layer of liquid, two related phenomena occur because of the local rise in temperature. The refractive index of the liquid will be changed by the heat, inducing a thermal defocusing or blooming effect which enlarges the beam and modifies its shape.[37] This optical effect is accompanied by a change in surface tension of the liquid layer, which induces thermocapillary or Bénard−Marangoni convection currents. These two effects result in a very fast liquid flow away from the center of the laser beam and the formation of a depression surrounded by a ridge in the liquid layer.[38] This explains the solution droplet's expansion. Additionally, since the solvent is simultaneously evaporated, a concentration gradient is induced and convection will eventually change from thermocapillary to concentration convection.[38] Meanwhile, the precursor crystals in solution and on the substrate surface react, and ZnO starts to nucleate. The IR photons also induce nondissociative multiphonon vibrational excitations that will relax through collisions in the molecular neighborhood's rotational and translational degrees of freedom.[39]

These very peculiar conditions set the solution/precursor system in a nonequilibrium state during the laser irradiation. This nonequilibrium state promotes the fast decomposition of precursor molecules to produce ZnO nanostructures, which would not be formed in oven heating at the same temperature

---

(24) Wu, J. J.; Liu, S. C. *Adv. Mater.* **2002**, *14*, 215.
(25) Yuan, H.; Zhang, Y. *J. Cryst. Growth* **2004**, *263*, 119.
(26) Shen, X.-P.; Yuan, A.-H.; Hu, Y.-M.; Jiang, Y.; Xu, Z.; Hu, Z. *Nanotechnology* **2005**, *16*, 2039.
(27) Kamata, K.; Nishino, J.; Ohshio, S.; Maruyama, K. *J. Am. Ceram. Soc.* **1994**, *77*, 505.
(28) Liu, J. F.; Bei, Y. Y.; Wu, H. P.; Shen, D.; Gong, J. Z.; Li, X. G.; Wang, Y. W.; Jiang, N. P.; Jiang, J. Z. *Mater. Lett.* **2007**, *61*, 2837.
(29) Kubota, J.; Haga, K.; Kashiwaba, Y.; Watanabe, H.; Zhang, B. P.; Segawa, Y. *Appl. Surf. Sci.* **2003**, *216*, 431.
(30) Rudolph, G.; Henry, M. C. *Inorg. Chem.* **1964**, *3*, 1317.
(31) Fiddes, A. J. C.; Durose, K.; Brinkman, A. W.; Woods, J.; Coates, P. D.; Banister, A. J. *J. Cryst. Growth* **1996**, *159*, 210.
(32) Arii, T.; Kishi, A. *J. Therm. Anal. Calorim.* **2006**, *83*, 253.
(33) Wolbarsht, M. L. *IEEE J. Quantum Electron.* **1984**, *QE-20*, 1427.
(34) Holbrook, K. A.; Oldershaw, G. A.; Shaw, C. J. *Int. J. Chem. Kinet.* **1993**, *25*, 323.
(35) Hong, R.; Wei, C.; He, H.; Fan, Z.; Shao, J. *Thin Solid Films* **2005**, *485*, 262.
(36) Lax, M. *J. Appl. Phys.* **1977**, *48*, 3919.
(37) Inaba, H.; Ito, H. *IEEE J. Quantum Electron.* **1968**, *QE-4*, 45.
(38) Nizovtsev, V. V. *J. Appl. Mech. Tech. Phys.* **1989**, *30*, 132.
(39) Danen, W. C. *J. Am. Chem. Soc.* **1979**, *101*, 1187.

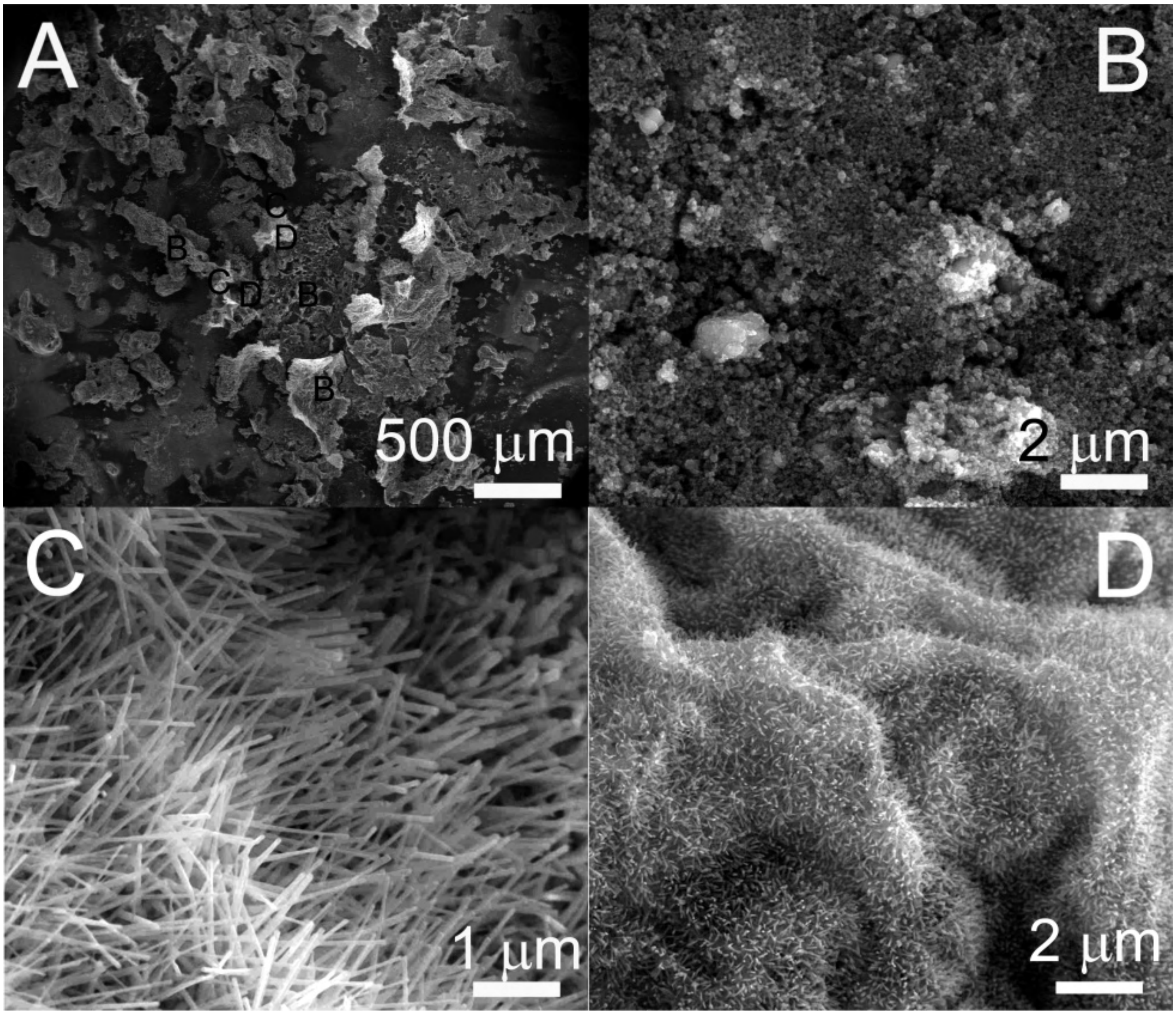

Figure 2. (A) Low-magnification view of deposit grown at 20 W, 2 s; (B) nanoparticle film; (C) nanowires; and (D) nanorods grown at the same parameters.

unless the oven heating was prolonged for many hours.[29] Indeed, the constraints for chemical reactions to proceed are often relieved under laser heating, allowing the reactions to occur at a much lower temperature than with standard heating.[40] The convection-induced fast transport of building blocks to the growing ZnO crystals can also increase the growth rate.

General Morphology of Deposits. Figure 2A shows a low magnification view of the center of a deposit (20 W, 2 s). Mounds of indeterminate shape with a very rough surface have grown in the center. The convection-induced deformation and mixing of the solution droplet is most likely responsible for this type of morphology. The ridges and the holes can also be created by bubbles of solvent and acetylacetone trapped underneath the deposit surface that push and pierce the deposited layer. Around the center mounds, a flatter film can be seen, accompanied by chains of other mounds. This morphology is found until the edge of the deposit, where a ring of large $Zn(AcAc)_2$ crystals can be found.

If the magnification is increased, it is possible to distinguish different micro- and nanostructures (as indicated by corresponding letters on Figure 2A). As indicated on Figure 2A, nanoparticle aggregates (Figure 2B) arranged in the form of thin films, thick mounds, and distorted sheets forming holes (in the center) cover most of the deposited area. On ridges further away from the center, the mounds' surfaces are covered by dense areas of nanowires (aspect ratio >10, Figure 2C), nanorods (aspect ratio <10, Figure 2D), and a mix of other nanostructures such as thin hexagonal-shaped nanoplates and nanonails (see Figure 5).

The appearance of different types of nanostructures in the area roughly delimited by a circle of 1 mm near the center of the laser spot is symptomatic of the locally changing experimental conditions created by the Gaussian beam profile and the random distribution of $Zn(AcAc)_2$ crystals in the over-saturated precursor solution. At the beginning of the

---

(40) Mengjia, S.; Wengqian, Y.; Minqian, L.; Xiaopeng, F. *Appl. Phys. B: Lasers Opt.* **1988**, *45*, 83.

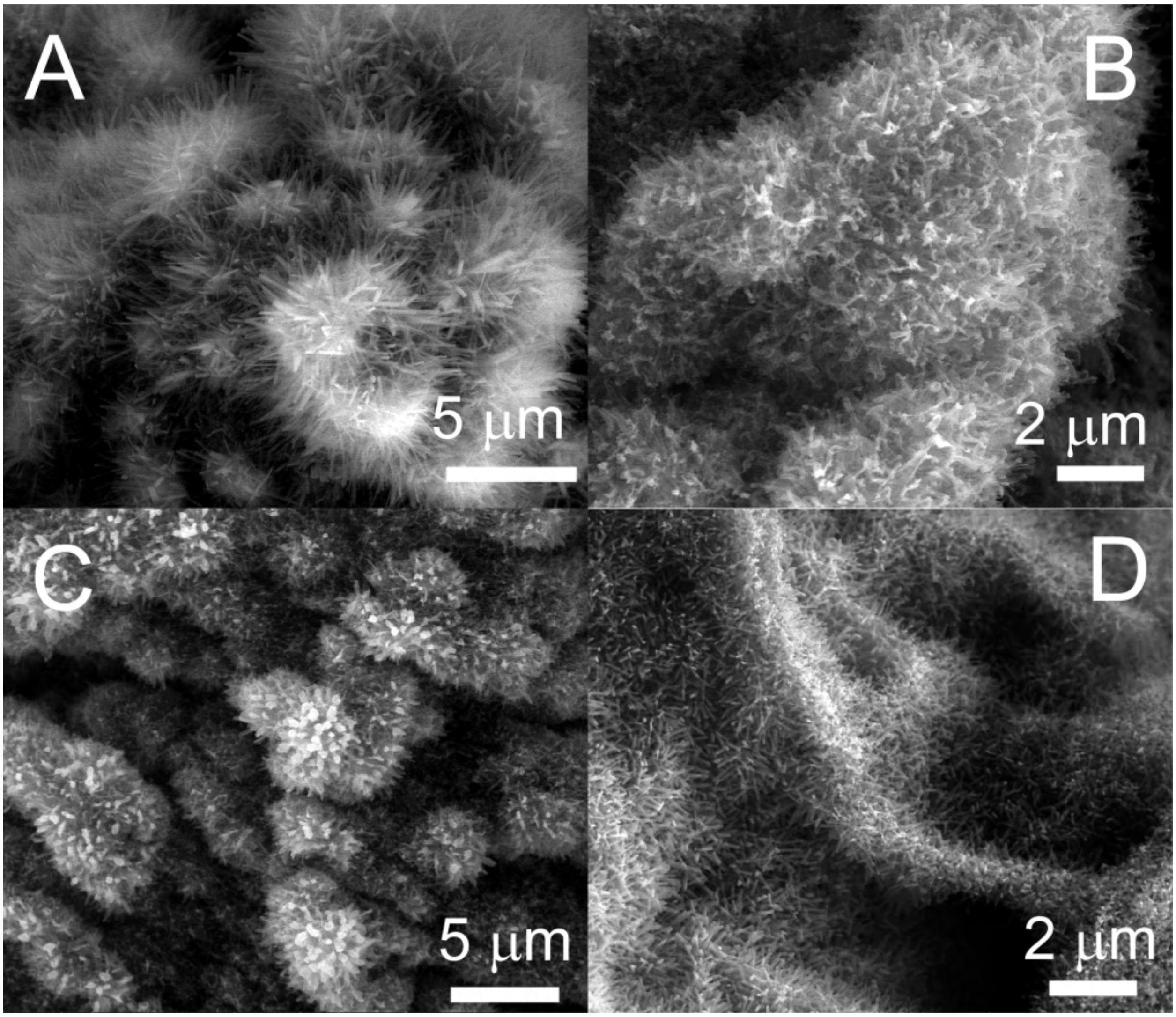

Figure 3. Influence of laser power on deposit morphology at a constant irradiation time of 10 s: (A) 5 W, 40 W/cm^2; (B) 10 W, 80 W/cm^2; (C) 15 W, 119 W/cm^2; (D) 20 W, 159 W/cm^2.

laser irradiation period, before the solvents are totally evaporated, the Zn(AcAc)$_2$ in the solution is decomposed and ZnO is homogeneously nucleated. The droplet's thickness quickly reduces, and the heterogeneous nucleation of randomly oriented nuclei starts on the glass substrate. This is probably why we have relatively flat films of ZnO nanoparticles grown on most of the substrate.

Conversely, since the solution was more a slurry than a clear solution, there were agglomerates of Zn(AcAc)$_2$ powder lying directly on the substrate. These precursor agglomerates also started to decompose into ZnO with a diminishing thickness of absorbing liquid above them and probably formed the mounds observed on the substrate. Since it is more energetically favorable than heterogeneous nucleation on a non-lattice-matched substrate,[41] the majority of nanostructure growth occurred on these uneven mounds by homoepitaxy. Also, given that the small ZnO nuclei formed by homogeneous nucleation in the first second of irradiation are more soluble than the bigger mounds, they probably migrated toward the growing mounds to attach themselves to ZnO crystals growing by homoepitaxy.

Influence of Laser Parameters on Morphology and Microstructure. Laser Power. IR laser light is the sole source of energy for precursor molecule dissociation, ZnO nucleation, and subsequent assembly into various nanostructures. Laser intensity will thus have much influence on the final product morphology and structure. Representative SEM pictures of the center region of samples grown at increasing laser powers and a constant irradiation time of 10 s can be seen in Figure 3. If no laser light is shone on the solution, the solvent eventually evaporates after a couple of hours and leaves behind the characteristic crystals and precipitated filaments of Zn(AcAc)$_2$ (not shown). At a power of 5 W (Figure 3A), the substrate is covered by mounds of flat crystalline whiskers. The whiskers have an average length of 1.3 μm (number of measurements, $N = 14$, standard deviation, $\sigma = 0.1$ μm) and an average width of 167 nm ($N = 9$, $\sigma = 25$). The whiskers buckle under low acceleration voltage (5 kV) in the SEM and contain approximately 46% C, 36% O, and 14% Zn according to EDS quantitative

---

(41) Yoon, S.; Kim, D. J. *J. Cryst. Growth* **2007**, *303*, 568.

measurements (±5% accuracy). It is safe to say that these whiskers are not ZnO but are recrystallized $Zn(AcAc)_2$ or an intermediary compound.

With a power of 10W (Figure 3C), more randomly grown ZnO whiskers can be seen (46% O, 54% Zn from EDS). The whiskers are smaller (average length = 759 nm with $N = 8$ and $\sigma = 111$, average width = 106 nm with $N = 19$ and $\sigma = 18$), and this shrinkage can be explained by the shedding of the AcAc ligand from the material, which has been observed in the organic-to-inorganic conversion of $Zn(AcAc)_2$ in superheated steam.[42] At 15 W (Figure 3C), the whiskers have a more defined shape (53% O, 47% Zn) with an average width of 297 nm ($N = 30$, $\sigma = 50$) and length of 852 nm ($N = 6$, $\sigma = 82$). Finally, at 20 W (Figure 3D), we see the appearance of well-defined ZnO nanorods on a large area of the deposit (49% O, 51% Zn). The nanorods of Figure 3D have an average length of 470 nm ($N = 25$, $\sigma = 75$) and width of 80 nm ($N = 45, \sigma = 12$). According to these results, surface $Zn(AcAc)_2$ was transformed into ZnO at laser intensities superior or equal to 80 W/cm^2 (10 W) but well-formed films of nanorods can only be found at 159 W/cm^2.

Irradiation Time. Samples were also grown at constant laser power but at varying irradiation time. To minimize the burning of the deposits, the samples were grown at lower irradiation times. Figure 4 shows typical SEM pictures of nanorods produced at a laser power of 20 W with two different irradiation times, 2 s (4A) and 5 s (4B). The nanorods cover an area of several square micrometers. The rods grown with an irradiation time of 2 s are much shorter (lengths between 100 and 200 nm) than the rods grown with an irradiation time of 5 s (lengths between 1 and 2 μm). The average widths of the rods grown for 5 s (311 nm, $N = 31$, $\sigma = 23$ nm) and for 2 s (46 nm, $N = 97$, $\sigma = 5$ nm) are also quite different. However, they both clearly have a hexagonal cross section, which might indicate growth along the [0001] direction of the hexagonal lattice of zinc oxide. The rods of Figure 4A have better vertical alignment than those from Figure 4B as the result of growth on a locally more level surface on the mound. Some rods grown with an irradiation time of 2 s are also fused or branched. This is because they are very short and have just emerged from the ZnO seed film or nucleation surface underneath. The scarcity of ZnO building blocks will promote the growth in only one direction or branch if it proceeds further.

ZnO nanowires were observed further away from the center of the reaction zone (~100 μm). The length of the wires grown at 20 W for 5 s can be appreciated in Figure 5A (average visible length of 4.4 μm, $N = 24$, $\sigma = 0.6$ μm). Figure 5B allows the measurement of their width (average width of 47 nm, $N = 26$, $\sigma = 3.7$ nm) and their average aspect ratio (aspect ratio = 94). The growth is much less uniform for shorter irradiation times, as shown in Figure 5C and D. Nanoplates (flat hexagonal plates) and nanonails (tip larger than body) with hexagonal tips between 100 and 300 nm wide are visible in Figure 5C while an assortment of nanowire derivations such as tapered nanowires and nanonails can be observed in Figure 5D. This is symptomatic of local variations in ZnO building blocks concentration during growth.

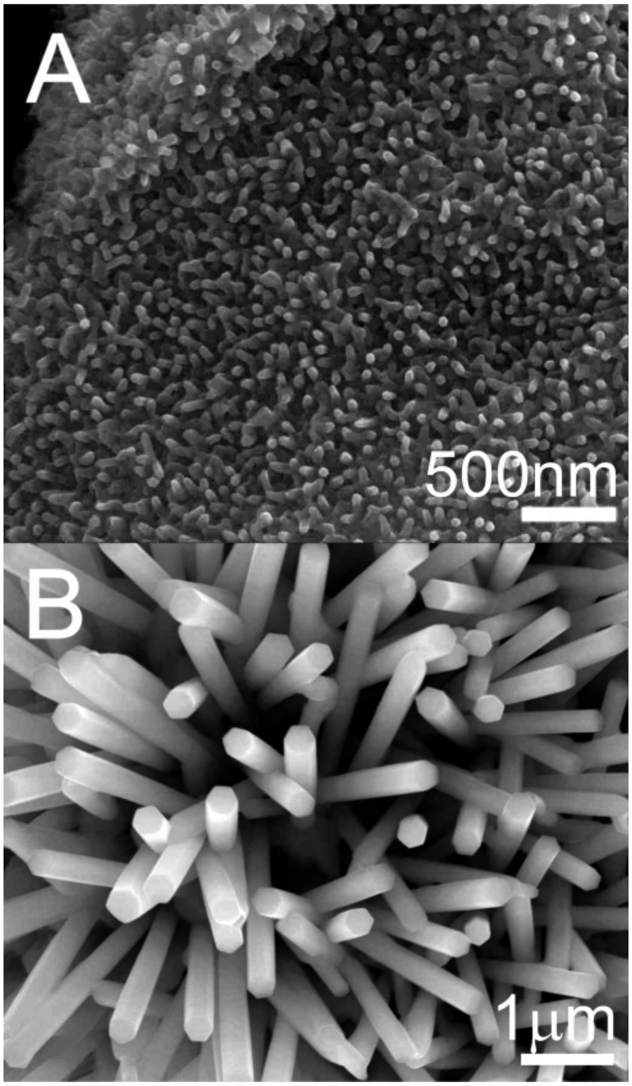

Figure 4. SEM images of nanorods with different laser irradiation parameters: (A) 20 W, 2 s; (B) 20 W, 5 s.

A shorter irradiation time led to the appearance of nanostructures that had not been observed in the samples grown at 10 s. It would seem that even though a longer irradiation time improves the overall crystallinity of the samples, the ensuing flame destroys or inhibits the growth of longer and more defined nanostructures. As a general trend, the nanowires and nanorods grown for 5 s are longer, more uniform (e.g., fewer diameter and morphology variations), and have more defined hexagonal cross sections than the nanostructures grown for 2 s. A slightly longer irradiation time gives rise to a more uniform heating field, produces more ZnO building blocks, and allows for more laser annealing. All these factors contribute to the growth of longer nanostructures.

XRD Analysis. X-ray diffraction patterns were obtained from two sets of samples. The first set of patterns shown in Figure 6A compares the structure of the ZnO films produced at different laser powers (10−30 W) for a constant irradiation

---

[42] Shishido, T.; Yubuta, K.; Sato, T.; Nomura, A.; Ye, J.; Haga, K. *J. Alloys Compd.* **2007**, *439*, 207.

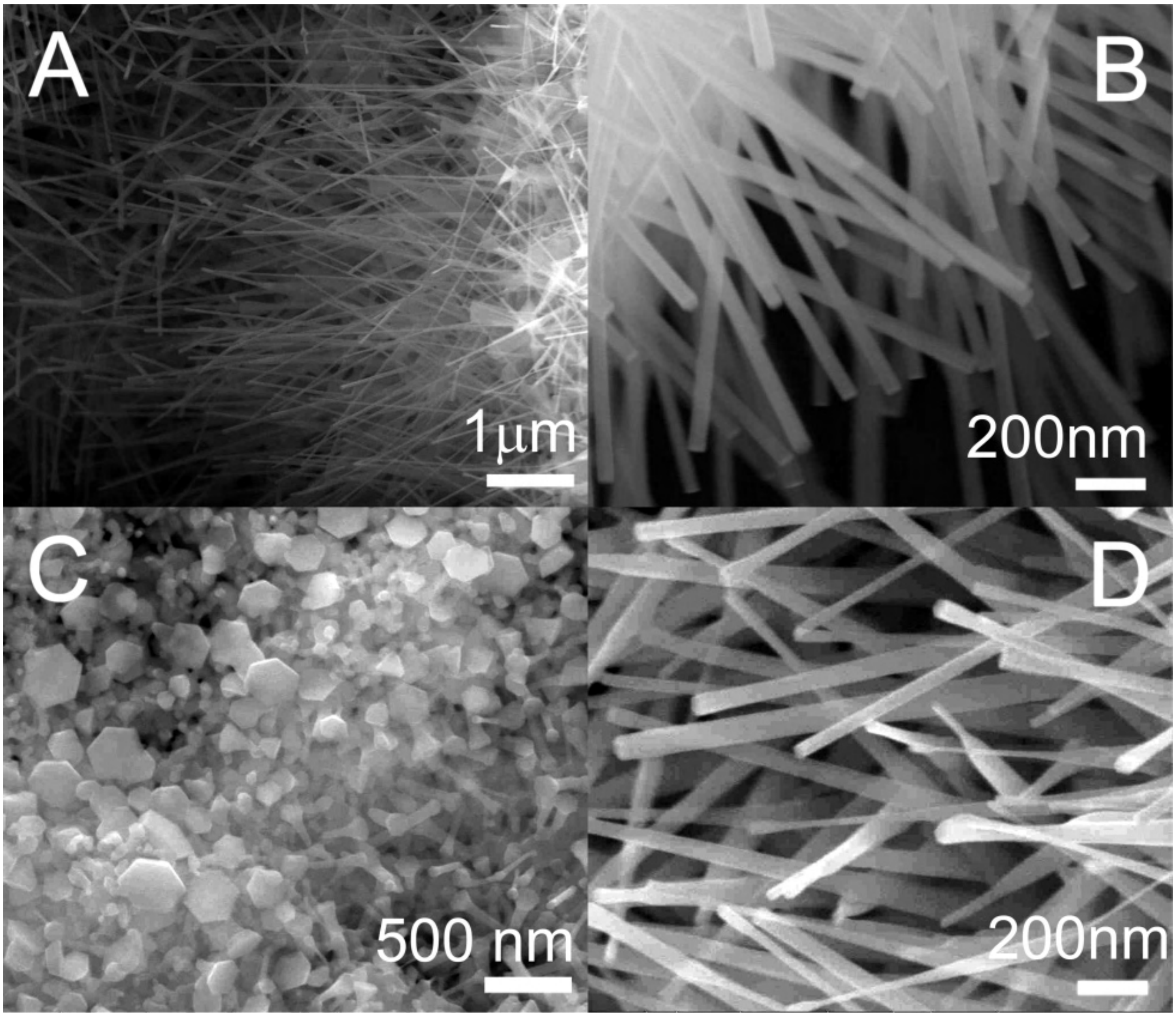

Figure 5. SEM images of nanowires and nanonails grown with different laser irradiation parameters: (A and B) 20 W, 5 s; (C and D) 20 W, 2 s.

time of 10 s. The as-is precursor and the air-dried solution patterns are also presented for comparison purposes. The second set shown in Figure 6B compares the structure of three ZnO films produced at different irradiation times (2−10 s) with a constant laser power of 20 W.

The main peaks observed for most samples are at $2\theta =$ 32°, 34°, 36°, 48.0°, 57°, 63°, 67°, 68°, and 69°. By assuming that the ZnO films have a hexagonal wurtzite structure and by comparing the peak positions to the reference values,[43] the following Miller indices were assigned to each peak: (100), (002), (101), (102), (110), (103), (200), (112), and (201), respectively. Overall, the recorded peak intensities slightly differed with those of the reference card intensities. Yet, no significant preferred orientation along any one direction was found. Indeed, the XRD signal originates from the whole sample, which is dominated by randomly oriented nanoparticles, as was confirmed with the SEM observations.

From Figure 6A, the three strongest peaks for $Zn(AcAc)_2 \cdot H_2O$ are centered at 18.5°, 24.5°, and 25.6°. Assuming the organic precursor is monoclinic, these three peaks would correspond to the (100), ($\bar{1}01$), and (101) planes for zinc bis(acetylacetonate) hydrate.[44] Similar features are present on the air-dried solution's pattern. Indeed, the three strongest peaks occur at 18.8°, 24.5°, and 25.5°. Three other peaks become apparent at 31.7°, 34.3°, and 36.2°. At this stage, the precursor is structurally different, presumably due to the evaporation of ethanol and water at room temperature and subsequent recrystallization from solution. Still, these peaks can be associated to the (002), ($\bar{1}02$), and (011) planes in $Zn(AcAc)_2$.

As the solution is irradiated with a laser set at 5 W, the peaks at 18.5° and 24.5° are still present but are broader. The three other peaks at 31.7°, 34.3°, and 36.2° intensify. This indicates that we may have an unknown intermediary compound or that small quantities of ZnO can be formed this low temperature. At 10 W, most of the characteristic $Zn(AcAc)_2$ peaks within the 18−30° interval disappear, whereas the peaks at 31.7°, 34.3°, and 36.2° become dominant. This would indicate that a ZnO film is formed.

---

[43] JCPDS card 36-1451, ZnO.

[44] JCPDS card 41-1634, zinc bis(acetylacetonate) hydrate.

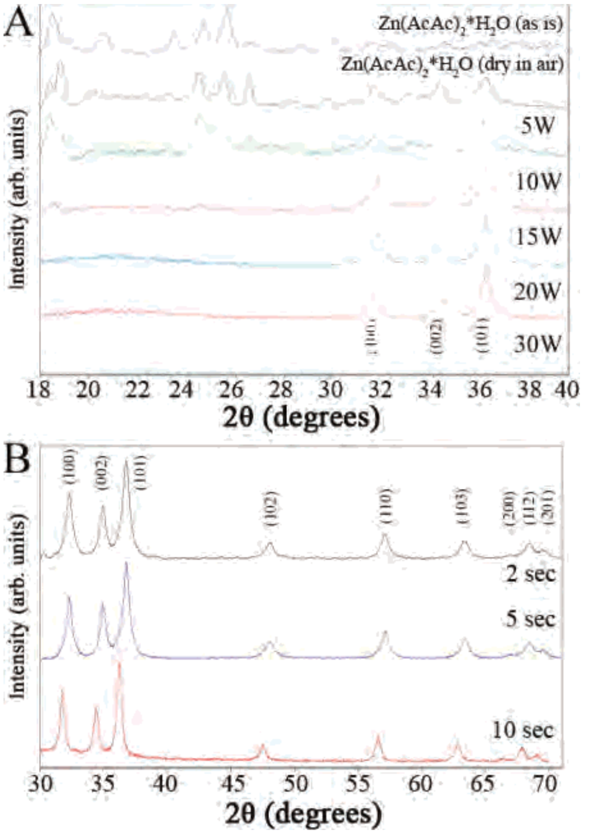

Figure 6. (A) XRD patterns of the ZnO films produced at different laser powers for a constant irradiation time of 10 s; (B) XRD patterns of the ZnO films produced at different irradiation times for a constant power of 20 W.

These dominant peaks would represent the (100), (002), and (101) planes, respectively, in hexagonal ZnO. As the laser power is further increased, the dominant peaks narrow, indicating that larger crystallites are grown.

The average grain size of the ZnO films can be estimated with Scherrer's equation from the diffraction peak's width at half its maximum intensity.[45] The average crystallite sizes were estimated to be 11.6, 12.2, 19.4, and 34.1 nm for the 10, 15, 20, and 30 W samples, respectively, using the (101) peak at 36°. Similarly, from Figure 6B, the main peaks narrow as irradiation time is increased. The crystallite sizes here were estimated to be 14.5, 16.0, and 21.0 nm for irradiation times of 2, 5, and 10 s, respectively. The crystallite size thus appears to increase with increasing laser power and increasing irradiation time. Also, some patterns have their main peak positions shifted by +0.5°, such as the 30 W sample in Figure 6A and the 2 and 5 s samples in Figure 6B. Strain in the crystal lattice has an effect on the diffraction peaks. Uniform strain leads to a peak position shift whereas nonuniform strain causes peak broadening.[45] Hence, there appears to be some uniform strain in some samples. The strain, as the porosity of the deposits, is caused by the simultaneous vaporization of solvent, decomposition of precursor, and crystallization of ZnO during laser irradiation.[46]

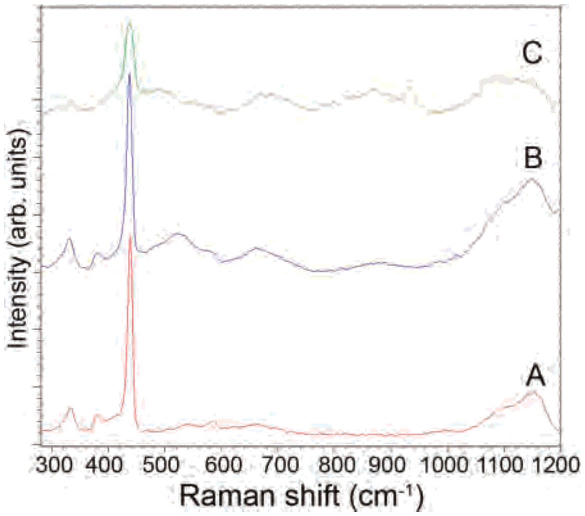

Figure 7. Raman spectra of: (A) ZnO commercial powder; (B) ZnO nanorods (20 W, 5 s); and (C) ZnO nanoparticles (20 W, 2 s).

Raman Spectroscopy Analysis. The samples were thoroughly examined using a microRaman spectroscope to obtain further information on their microstructure. The probing laser was aimed at an area of the sample where, based on previous SEM observation, it was known that specific types of nanostructures had been deposited. Commercial ZnO powder was first analyzed to provide a reference spectrum (curve in Figure 7A). The majority of the reported features for bulk ZnO are visible on the spectrum with the A_1 TO (transverse optical) mode at 380 cm^{-1}, the E_1 TO mode at 414 cm^{-1}, the E_2 H (high) mode at 438 cm^{-1}, the A_1 LO (longitudinal optical) mode at 579 cm^{-1}, and the E_1 LO mode at 585 cm^{-1}.[47,48] The other features, such as the peaks at 331 cm^{-1} (A_1 acoustic overtone), 1106 cm^{-1}(A_1, E_2 acoustic combination), and 1156 cm^{-1} (A_1 optical combination), are second order in nature, resulting from various combinations and overtones.[49]

The spectrum taken in a ZnO nanorod-rich area (curve in Figure 7B) is similar to the reference (A_1 TO at 381 cm^{-1}, E_1 TO at 420 cm^{-1}, E_2 H at 436 cm^{-1}, and A_1 LO at 578 cm^{-1}) but features slightly broader peaks. The high intensity and low width of the E_2 peak is symptomatic of a large crystallite size. The E_1 LO peak is absent or too small to be detected, indicating that very few oxygen vacancies are present along the *c* axis.[49,50] Small defect-related peaks appear at 505 and 870 cm^{-1}.[51,52] There is also an additional peak at 471 cm^{-1} that can be attributed to the Si−O−Si symmetric stretch of the quartz substrate.[53]

---

(45) Cullity, B. D. *Elements of X-ray Diffraction*, 2nd ed.; Addison-Wesley: Reading, MA, 1978.

(46) Ohyama, M.; Kozuka, H.; Yoko, T. *Thin Solid Films* **1997**, *306*, 78.

(47) Damen, T. C.; Porto, S. P. S.; Tell, B. *Phys. Rev.* **1966**, *142*, 570.

(48) Arguello, C. A.; Rousseau, D. L.; Porto, S. P. S. *Phys. Rev.* **1969**, *181*, 1351.

(49) Wang, R. P.; Xu, G.; Jin, P. *Phys. Rev. B: Condens. Matter Mater. Phys.* **2004**, *69*, 113303.

(50) Wei, X. Q.; Man, B. Y.; Liu, M.; Xue, C. S.; Zhyang, H. Z.; Yang, C. *Physica B (Amsterdam, Neth.)* **2007**, *388*, 145.

(51) Xing, Y. J.; Xi, Z. H.; Xue, Z. Q.; Zhang, X. D.; Song, J. H.; Wang, R. M.; Xu, J.; Song, Y.; Zhang, S. L.; Yu, D. P. *Appl. Phys. Lett.* **2003**, *83*, 1689.

(52) Dong, Z. w.; Zhang, C. F.; Deng, H.; You, G. J.; Qian, S. X. *Mater. Chem. Phys.* **2006**, *99*, 160.

(53) Williams, Q. *AGU Handbook of Physical Constants*; Ahrens, T. J., Ed.; American Geophysical Union: Washington, DC, 1995; Vol. 2, p 291.

The spectrum taken in a ZnO nanoparticle-rich area (curve C) is noisier and presents broader and less defined features compared with those of the bulk and nanorod spectra. The main peaks are present (A_1 TO at 388 cm^{-1}, E_1 TO at 418 cm^{-1}, E_2 H at 437 cm^{-1}), but the two LO peaks are lost behind defect-induced peaks at 505, 553, and 867 cm^{-1}. Lower A_1 and E_2 peak intensities confirm that the crystallite size of the ZnO nanoparticles is lower than that for the ZnO nanorods.[49,54] The signal from the quartz substrate (wide peak at 473 cm^{-1}) might hide other peaks since the particles are smaller and do not cover the substrate as well as the nanorods (porous thin film). The peak at 553 cm^{-1} results from incomplete Zn oxidation or interstitial Zn atoms.[51] The peak around 935 cm^{-1} probably arises from the C−C stretch in $Zn(AcAc)_2$ or one of its decomposition products.[55] This confirms the partial reaction in the periphery of the irradiation zone because of a lower temperature.

Crystal Growth. Figure 8 shows a high-magnification TEM image of the ZnO nanorods. A 130 nm wide rod grown at 20 W for 5 s is presented in Figure 8A. The inset of Figure 8A is the SAED pattern of the rod, showing that the rod is a single crystal. Indeed, three *d* values (interplanar distances) were measured on the diffraction pattern, $d_1 = 5.12$ Å, $d_2 = 2.78$ Å, and $d_3 = 2.46$ Å, which allowed three diffraction spots on the pattern to be indexed using known values for hexagonal ZnO.[43] With the [001] and [100] directions in the pattern, the zone axis can only be [010]. The occurrence of the 001 reflection is interesting, considering that it is normally a forbidden reflection. Like the 003 spot, the 001 spot arises from double diffraction, in this case, a combination of 011 and $0\bar{1}0$ diffraction.[56] If the [001] direction is transferred on the image, it can be deduced that the rod has grown along the [001] or *c* axis direction of the hexagonal wurtzite lattice. This was expected, since the fastest growth direction for the polar ZnO crystal is along the *c* axis or [001] direction.[21,57] The same can be said of the rod displayed in Figure 8B (30 W, 10 s) where the (001) lattice fringes can be distinguished (interfringe distance = 5.23 Å which corresponds to the *c* axis with an error of 0.4% from the reference value[43]) and are perpendicular to the growth direction. The corresponding diffraction pattern (inset of Figure 8B) was taken in the same zone axis (010) as that of Figure 8A, and similar *d* values were measured ($d_1 = 5.15$ Å, $d_2 = 2.79$ Å, and $d_3 = 2.46$ Å). The surfaces are remarkably flat, with only a few atomic layers of roughness on the hexagonal-shaped tip and sides.

An EDS spectrum was taken on the tip of a nanorod during the TEM observations (not shown). Besides the signals from the beryllium window near the origin and the copper grid (a shoulder on the L peak of Zn and a peak at around 8 keV), only Zn and O were detected. Quantification using the commercial ZnO powder as a reference sample and by correcting for absorption (μ/ρ mass absorption coefficients from Goldstein et al.[58]) confirmed the ZnO 1:1 stoichiometry. This indicates that if there are impurities or intermediary compounds involved the early stage of the growth process, they are not present in the fully grown nanorods.

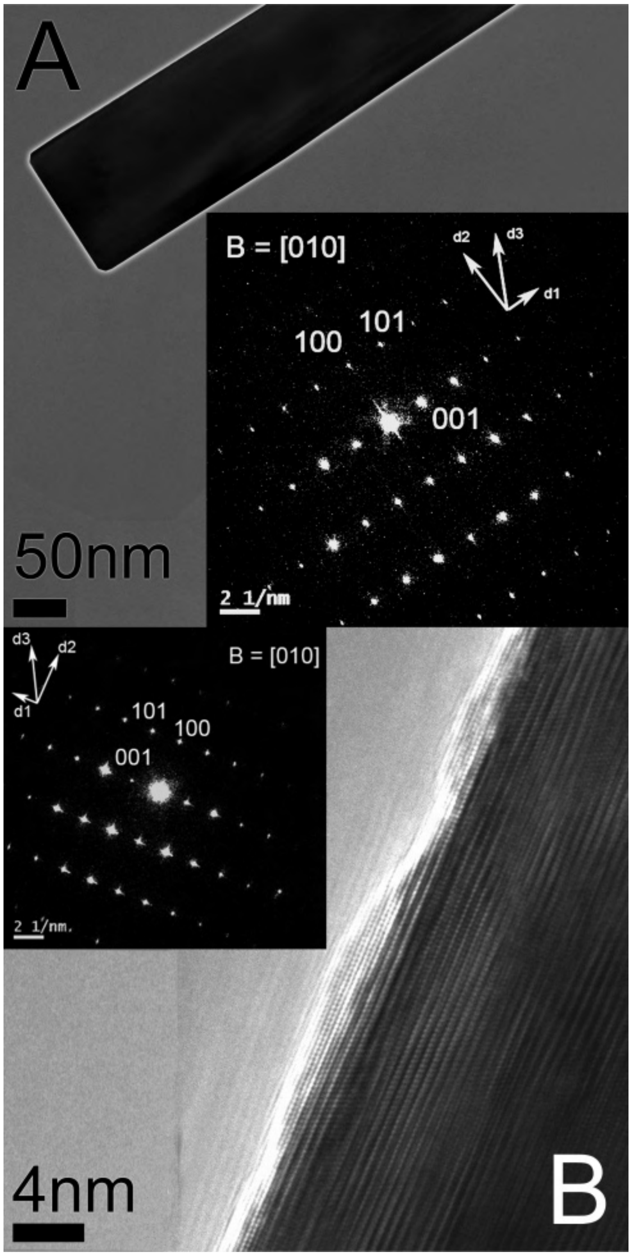

Figure 8. TEM images and SAED patterns of nanorods: (A) 20 W, 5 s; and (B) 30 W, 10 s.

There are two general models for the growth of crystals in a supersaturated medium: Ostwald ripening, where the growth of larger crystals from smaller crystals is promoted because of mass transport mechanisms and solubility differences, and a more recently discovered mechanism called

---

(54) Rajalakshmi, M.; Arora, A. K.; Bendre, B. S.; Mahamuni, S. *J. Appl. Phys.* **2000**, *87*, 2445.

(55) Nakamoto, K. *Infrared and Raman Spectra of Inorganic and Coordination Compounds: Part B*, 5th ed.; Wiley-Interscience: New York, 1997.

(56) Hirsch, P. B.; Howie, A.; Nicholson, R. B.; Pashley, D. W.; Whelan, M. J. *Electron Microscopy of Thin Crystals*, 1st ed.; Butterworth & Co.: London, 1967.

(57) Li, W. J.; Shi, E. W.; Zhong, W. Z.; Yin, Z. W. *J. Cryst. Growth* **1999**, *203*, 186.

(58) Goldstein, J. ; Newbury, D. E.; Joy, D. C.; Lyman, C. E.; Echlin, P.; Lifshin, E.; Sawyer, L. C.; Michael, J. R. *Scanning Electron Microscopy and X-ray Microanalysis*, 3rd ed.; Kluwer Academic/Plenum Publishers: New York, 2003.

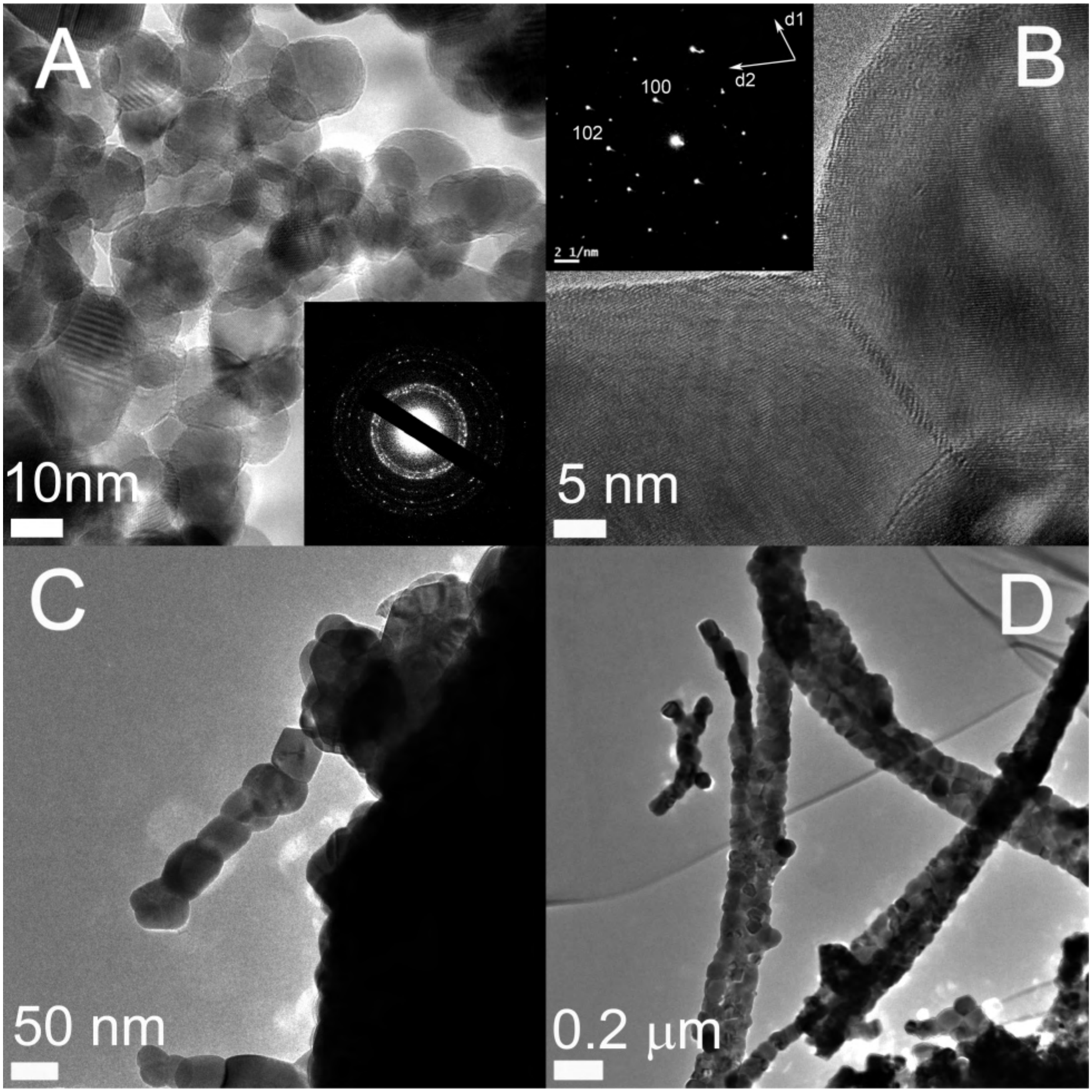

Figure 9. TEM images and SAED patterns of ZnO nanoparticles and assemblies produced with different laser irradiation parameters: (A) 15 W, 10 s; and (B−D) 20 W, 2 s.

"oriented attachment" where small particles aggregate to form a rodlike solid by self-assembly.[59] According to the latter model, the particle aggregates have the appearance of pearl chains and linearly aggregate to form a rod when the crystal surfaces have different surface energies such as in the wurtzite ZnO crystal. Once aggregated, the nanoparticles undergo spontaneous adjustment and the adjacent crystallographic planes fuse.[60] Since, according to recent modeling studies, coalescence by Ostwald ripening takes place on a larger time scale than that of oriented attachment, we believe that it is the latter growth mechanism which is mostly responsible for the growth of the nanostructures presented in this study.[61]

Indeed, ZnO nanoparticles in different stages of crystal growth and assembly cover most of the reaction zone. The HRTEM picture of Figure 9A shows the particles with an average size of 16 nm ($N = 42$, $\sigma = 3$ nm) and with spherical, polygonal, or oblong shapes. The SAED pattern in the inset of Figure 9A can be indexed with the *d* values of wurtzite ZnO and shows that the particles have many different crystal orientations, producing a pattern of incomplete diffraction rings. These randomly oriented but single-crystal nanoparticles appear to be the ZnO building blocks

---

[59] Pacholski, C.; Kornowski, A.; Weller, H. *Angew. Chem., Int. Ed.* **2002**, *41*, 1188.

[60] Zhang, Y.; Lu, F.; Wang, Z.; Zhang, L. *J. Phys. Chem.* **2007**, *111*, 4519.

[61] Ethayaraja, M.; Bandyopadhyaya, R. *Langmuir* **2007**, *23*, 6418.

and will assemble in larger structures to form the nanorods and nanowires previously observed.

Figure 9B shows a close-up view of two aggregated particles in the process of oriented attachment. The lattice fringes are visible on both particles and feature the same interfringe distance of 2.9 Å, which corresponds to the 100 interplanar distance. A dislocation is visible where the two particles merge. The diffraction pattern in the inset of Figure 9B confirms the previous assessment, with $d_1 = 2.74$ Å and $d_2 = 1.85$ Å, which are values near the reference values of $d_{100} = 2.81$ Å and $d_{102} = 1.91$ Å.[43] The area selection diaphragm was set mainly on the left particle, but part of the right particle must have been covered by the diaphragm since multiple faint diffraction spots are visible. Further controlled inclining of the sample is required to identify the zone axis. Figure 9C shows a small linear pearl-chain aggregate of six particles connected to each other by a crystal face which is attached to a larger aggregate of particles. Similar linear pearl-chain ZnO particle aggregates have recently been observed by Yubuta et al., who were also studying the water-enhanced pyrolysis of $Zn(AcAc)_2$ hydrate.[62]

Rodlike structures approximately three particles wide are shown in Figure 9D as further evidence of the oriented attachment crystal growth. It is believed that the gaps between the particles are filled and the crystal surfaces parallel to the *c* axis are smoothened by the conventional Ostwald ripening coalescence process, which assists oriented attachment.[59] This could be the case in our situation, but the process is probably too fast for this to happen in the conventional manner.[61] Laser annealing and/or convection must enhance building block mobility for long, smooth, and hexagonal rods such as those of Figure 4A to grow in 5 s.

Improving Selectivity and Reproducibility. This type of laser-assisted ZnO synthesis route is quite new. The aim of this paper is to report the most recent results obtained and to illustrate this techniques' potential. To produce a variety of nanostructures on the substrates shows the possibilities of the process and simplifies its parametric characterization. For instance, because of the Gaussian-like laser-induced temperature gradient and resulting convection currents, different regions of the substrate are subjected to a different heat flux, giving insight into what could happen at a lower temperature or laser power density. Once the process is sufficiently characterized, the experimental parameters needed to produce specific nanostructure morphologies will be known and the selectivity improved.

Yet, using this method, reproducibility is limited. Indeed, many factors contribute to reduce control over the final product: The standard dropper used does not allow the delivery of precisely the same quantity of precursor solution each time; the $Zn(AcAc)_2$ powder aggregates in suspension are randomly distributed in the reaction zone, causing growth to be localized on mounds and on a generally uneven surface; and the laser beam's intensity profile induces a temperature gradient in the reaction zone, which may contribute to the instability of the heating process and the evaporation of the solvents.

As such, the precursor preparation methods will be improved in upcoming experiments in order to obtain reasonable yield, efficiency, and selectivity. For example, a homogeneous solution would allow the use of micropipettes, which would normally clog using the present solution, ensuring that a specific volume of solution is dropped for every experiment. The problems related to the initial random distribution of precursor particles on the substrate could also be corrected. This could be done by fine-tuning the precursor concentration to avoid over-saturating the solution, by adding acetic acid to the solution[63] or by choosing another solvent. A beam homogenizer could also be used to obtain a flat-top-type intensity profile, but such equipment reduces the laser beam power.

Conclusion

The fast synthesis of ZnO nanostructures by the laser-induced decomposition of zinc acetylacetonate in a solution of water and ethanol has been demonstrated. Nanorods, nanowires, and nanoparticles have been deposited on different regions of a fused quartz substrate by the irradiation of a CO_2 laser for a few seconds. The occurrence of the different types of ZnO nanostructures was found to be dependent on the laser power and irradiation time experimental parameters, which will have a direct effect on the morphology and crystal structure of the final deposits. A certain threshold laser power (10 W) was needed to produce a suitably high temperature for the complete decomposition of the precursor molecules. Once the laser power is sufficiently high, increasing the laser power enhances the crystallite size of the samples. Conversely, increasing laser irradiation time also increases crystallite size but can result in the destruction of the finer nanostructures because of laser annealing and combustion. Similarities were also observed between hydrothermal or aqueous chemical synthesis and laser thermochemistry at the crystal growth level even though the processing times used here are shorter by several orders of magnitude.

The lack of deposit homogeneity resulting from the Gaussian beam profile, although usually unwanted, remains interesting since it represents different deposition regimes that can be further investigated. From the experimental point of view, this allows the study of different growth regimes with a limited number of experiments. Combining the advantages of conventional chemical processing and MOCVD, with a low processing temperature and a cheap precursor, while being a much more straightforward and rapid process, laser-induced decomposition is thus a very promising technique for the deposition of a wide variety of ZnO nanostructures or other materials. Additionally, having the reaction occur in open air instead of in a reaction chamber or an autoclave greatly reduces processing times and

---

(62) Yubuta, K.; Sato, T.; Nomura, A.; Haga, K.; Shishido, T. *J. Alloys Compd.* **2007**, *436*, 396.

(63) Domansky, K.; Rose, A.; Grover, W. H.; Exarhos, G. *J. Mater. Sci. Eng. B* **2000**, *B76*, 116.

experimental setup complexity while keeping the operational costs low. Further research will aim for structure-selective synthesis by the optimization of laser and precursor solution parameters.

Acknowledgment. The authors gratefully acknowledge funding for this project by the Natural Sciences and Engineering Research Council of Canada and the Canadian Foundation for Innovation. Financial support for C.F. and R.L. was provided by the government of Québec (Fonds Québécois de la Recherche sur la Nature et les Technologies). The authors also thank Jean-Philippe Masse and Monica Nelea for help with characterization and Ramkiran Godug-uchinta for laser interface *Labview* programming.

IC700915Z